Critical scaling of the ac conductivity and momentum dissipation

Nikolaos Angelinos,[1] Elias Kiritsis,[2] and Francisco Peña-Benitez[3]
[1]*Department of Physics, University of Kentucky, Lexington Kentucky, USA*
[2]*Universite de Paris, CNRS, Astroparticule et Cosmologie, F-75006 Paris, France and Crete Center for Theoretical Physics, Institute for Theoretical and Computational Physics, Department of Physics, P.O. Box 2208, University of Crete, 70013, Heraklion, Greece*
[3]*Max-Planck-Institut für Physik komplexer Systeme, Nöthnitzer Strasse 38, 01187 Dresden, Germany*

(Received 14 August 2020; revised 13 November 2020; accepted 16 November 2020; published 12 January 2021)

The scaling of the AC conductivity in quantum critical holographic theories at finite density, finite temperature, and in the presence of momentum dissipation is considered. It is shown that there is generically an intermediate window of frequencies in which the IR scaling of the AC conductivity is clearly visible.

DOI: 10.1103/PhysRevResearch.3.013028

I. INTRODUCTION AND SUMMARY

Critical behavior, scaling, and universality are landmarks that stand out from the messy reality of materials. It is well known that criticality and scaling can appear in both weakly coupled and strongly coupled theories. In the first case the simplest scale invariant theories are free massless theories and are obviously very easy to handle. Critical points at weak nonzero coupling are more rare to come by, as they need a special context for the β-function to vanish reliably in perturbation theory. Well-known examples are Wilson-Fisher fixed points in $d-\epsilon$ dimensions with $\epsilon \ll 1$ [1], and more nontrivial examples are found in the Banks-Zaks variety [2]. For strongly coupled theories, however, our tools have been so far anecdotal and usually consist of pushing the Wilson-Fisher idea to $\epsilon \sim 1$. A concrete example where quantum criticality, and scaling, may be realized, while the underlying theories are mostly strongly coupled, is in strange metals that include high-T_c superconductors [3–7]. The scaling of the direct current (DC) conductivity in the cuprates has been since the start one of the basic hallmarks, exhibiting linear resistivity at optimal doping over a large range of temperatures [8–14]. More recent and refined data on the DC conductivity in clean materials and a novel parametrization, indicated an unusual low-temperature asymptotic behavior and suggested the existence of a line of quantum critical points [11]. Similar evidence for a line of critical points was found in other cases [15,16], although this interpretation is contentious in the strange metal community.

The magnetoresistance of related materials has indicated also exotic behavior and a different scaling of the Hall angle in the overdoped regime [17–27]. New measurements of the magnetoresistance in strong magnetic fields also indicated scaling both in pnictides [28,29] and cuprates [30].

Studies of the alternating current (AC) conductivity [31] also produced scaling in ω in an intermediate range of frequencies. Although, it is typical for critical theories to induce a scaling in the AC conductivity in the far infrared (IR), it is unusual that such scaling should survive and be visible at higher frequencies. Further experiments showed similar scaling of the AC conductivity in other strange metals [32,33].

Despite the wealth of experimental indications of scaling phenomena in strongly coupled materials, progress in theory has been slower. The main reason is that few scale-invariant quantum critical points were known in two spatial dimensions and only one that is non-Gaussian. This has changed with the anti–de-Sitter/conformal field theory (AdS/CFT) correspondence [34], also known as holography. This emerged in string theory and provided a valuable tool in analyzing quantum field theories at strong coupling and was especially successful in describing scale invariant, strongly coupled theories at finite density. This has led to a classification of quantum critical behavior at strong coupling, as a function of the symmetries [35–39]. Moreover, holography provides techniques for calculating the quantum effective potential at finite density and temperature [40] that provides a powerful tool in studying phase transitions. A wide spectrum of condensed matter problems was addressed using these techniques, and this progress is summarized in reviews and lectures [41–44] as well as in books [45–48]. A recent overview of the progress in the field can be found in [49].

In the context of holography, studies indicated that the behavior of fermions and their correlations at strong coupling may be radically different from that at weak coupling [50,51]. This gave, in particular, a class of realizations of the marginal Fermi liquid [50], realizing correlators that were associated with the linear behavior of the DC conductivity [52]. Further holographic studies analyzed the constraints on the realization of a linear in T DC conductivity and provided explicit examples [53–55]. In particular, in [54], the model exhibits nonrelativistic $z=2$ Schrödinger symmetry and reproduces the $T+T^2$ behavior of the DC conductivity [11] and a Hall

angle and magnetoresistance that are in agreement with data at very low temperatures [21]. Moreover, it realized the idea of a line of quantum critical points, suggested in [11] and predicted scaling relations in the presence of the magnetic field.

The scaling properties in the presence of magnetic fields are nicely described by holographic critical theories. In general, charge dynamics is described by the Dirac-Born-Infeld (DBI) action, and its scaling analysis in the presence of magnetic fields has yielded a rich collection of scaling behaviors [54,56]. In one particular case, such a scaling behavior matches the one seen in the pnictides and cuprates [28–30].

The scaling of the AC conductivity observed in [31] has been tougher to crack. A conventional approach suggested that it may arise from the interaction of the fermions with a Bose sector other than the phonons [57]. In holography it has been studied since the authors of [35] observed that in scaling critical geometries there is also a scaling AC conductivity and computed the scaling exponent as a function of the other critical exponents for the case where the EM gauge boson is the same as the one that seeds the scaling IR geometry. This issue was further studied in [38] and more recently in [58]. It was then shown that one could also have intermediate regimes which also have scaling properties, and they may affect the intermediate scaling of the AC conductivity [59].

A definitive study was done in [60]. There, the model of [54] was analyzed by computing its AC conductivity in its various regimes. A related study of scaling was done in [61]. Furthermore, in [62,63], theories were studied where the AC conductivity was controlled by irrelevant deformations and where the scaling arguments are more complex to implement.

A. On the scaling of the holographic AC conductivity

In this section, we will briefly summarize the results found in [60] to set the framework for our current work.

The first theory that was analyzed in [60] was the holographic DBI theory of a strange metal, proposed in [54]. This theory has several parameters, but the physics depends only on two scaling variables t, that is proportional to the temperature, and J, that is proportional to the charge density. They both take all positive real values. The doping parameter is a combination of both scaling variables.

The $T + T^2$ behavior of the resistivity in [11] and the $T + T^2$ behavior of the inverse Hall angle, observed in [21] at *very low temperatures* $T < 30\,\mathrm{K}$, where a single scattering rate is present, were successfully described in this theory. The model is also in accord with the distinct origin of the criticality at very low temperatures advertised in [12], while the higher temperature, $T > 100\,\mathrm{K}$, scaling has different behaviors between the linear temperature resistivity and the quadratic temperature inverse Hall angle, signaling two scattering rates [22]. This regime in the model is different, however, from what experiments show about the cuprates.

In addition to the resistivity and inverse Hall angle, very good agreement was also found with experimental results of the Hall coefficient, magnetoresistance, and Köhler rule on various high-T_c cuprates [11,17–27]. The model provided also a change of paradigm from the notion of a quantum critical point, as it is quantum critical at $T \to 0$ on the entire

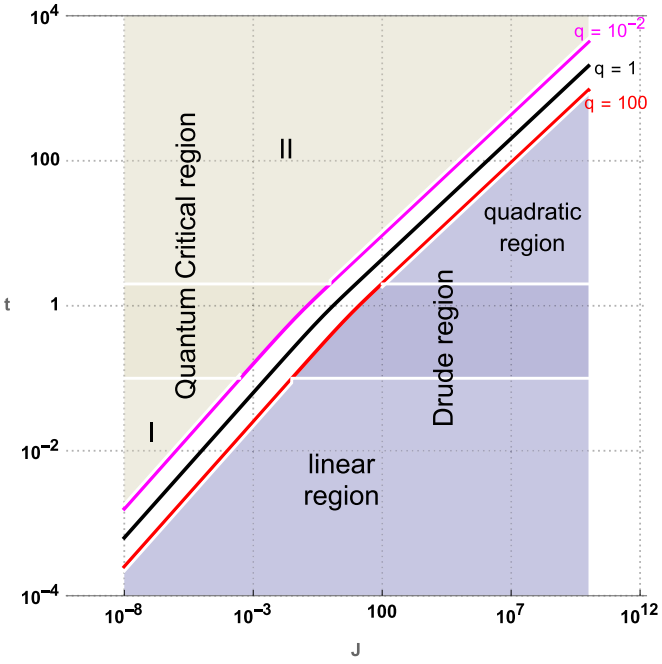

FIG. 1. The parameter landscape of the DBI Theory and the regimes for the DC conductivity. Figure reused from [60] under license https://creativecommons.org/licenses/by/4.0/.

overdoped region as suggested by the data found in [11]. The DC conductivity of this theory, as is usual in quantum critical theories, has two contributions [54]. One, which we call the Drude contribution, is related to momentum dissipation in the standard fashion, although here there are no weakly coupled quasiparticles. The other is independent of the momentum relaxing scattering time and survives at zero charge density and is the quantum critical contribution.[1]

There are two main regimes on the (t, J) plane. They are best described by a parameter q that is a function of t, J and distinguishes between the two regimes. When $q \gtrsim 1$ the DC conductivity is dominated by the Drude (drag) contribution. When $q \lesssim 1$ the DC conductivity is dominated by the quantum critical (QC) contribution. As the drag contribution to the conductivity is proportional to charge density, it follows that at zero charge density ($J = 0$) we are always in the QC/PP regime. These two regimes are shown in Fig. 1.

(1) In the Drude regime ($q \gg 1$), when $t \ll 1$ the resistivity is linear in t (and consequently in the temperature). This is the *linear regime*. When $t \gg 1$, the resistivity is quadratic in t. This is the *quadratic regime*.

(2) In the QC regime ($q \ll 1$), when $t \ll 1$, the resistivity behaves as $\rho \sim t^{-\frac{3}{2}}$. This is *regime I*. When $t \gg 1$ the resistivity behaves as $\rho \sim t^{-\frac{1}{2}}$. This is *regime II*.

In the $t \to 0$ limit the theory has an effective Lifshitz exponent $z = 2$ while as $t \to \infty$ it crosses over to an effective relativistic Lifshitz exponent $z = 1$ [54]. What we find in our analysis is as follows.

[1]This is also known as the Lindard continuum contribution.

(1) A *generalized relaxation time* τ can be defined by the IR expansion of the AC conductivity

$$\sigma(\omega) \approx \sigma_{DC}[1 + i\,\tau\,\omega + \mathcal{O}(\omega^2)]. \tag{1}$$

In the presence of a Drude peak, this is the conventional definition of an associated relaxation time. When there is no Drude peak present, τ is still well defined via (1), although in that case the interpretation as a relaxation time is lost.

In [60] an analytical formula for τ was given. It simplifies for large and small values of the scaling temperature variable t. In the regime I

$$\tau \sim \sqrt{t}, \tag{2}$$

while in the regime II (with $t \gg 1$) τ is set by the inverse of the temperature

$$\tau \simeq \frac{1}{t}. \tag{3}$$

(2) In the Drude regime ($q \gg 1$) where the dominant mechanism for the conductivity is momentum dissipation, there is a clear Drude peak in the AC conductivity.

In the QC regime there is no Drude peak and we have an incoherent AC conductivity.

(3) In the QC regime there is a scaling tail for the AC conductivity that behaves as

$$|\sigma| \sim \left(\frac{\omega}{t_{\text{eff}}}\right)^{-\frac{1}{3}}, \quad \text{Arg}(\sigma) \simeq \frac{\pi}{6}. \tag{4}$$

At finite charge density, this tail survives not only in the QC regime but also in parts of the Drude regime.

(4) This scaling tail of the AC conductivity, generalizes to more general scaling holographic geometries, as previously described in [35,38]. In this case, the theory was taken to have $T = 0$ and no momentum dissipation.

In particular, for a metric with Lifshitz exponent z, hyperscaling violation exponent θ, and conduction exponent ζ [37,38] with d spatial boundary dimensions, we find that, in general,

$$|\sigma| \sim \omega^m, \quad \text{Arg}(\sigma) \simeq -\frac{\pi\, m}{2}, \tag{5}$$

with

$$m = \left|\frac{z + \zeta - 2}{z}\right| - 1\,. \tag{6}$$

There are several constraints in the parameters of this formula that are detailed in [60]. This formula is valid when the associated charge density does not support the IR geometry. In this case the scaling exponent can become negative but is also $m \geqslant -1$.

(5) In the special case where the associated gauge field seeds the IR scaling geometry, the exponent m takes the value

$$m = \left|\frac{3z - 2 + d - \theta}{z}\right| - 1 \tag{7}$$

and is always positive.

(6) An important question is whether the scaling of the AC conductivity described above, for the general scaling geometries, is controlled by the dynamics of the charge density, or it is decided by the neutral system. What was found in [60] is that it is the neutral system that decides the exponent m. The charged contribution is almost always subdominant.[2]

The results of [60] have positively indicated that holographic QC theories at finite density and $T = 0$, in the absence of momentum dissipation, have a scaling IR AC conductivity, roughly of the type seen in experiments.

There is, however, an important difference, with the AC conductivity seen in experiments as one needs to turn on nonzero temperature and momentum dissipation and see to what extent this scaling survives these effects. It must also appear in the midfrequency range roughly $T \ll \omega \ll \mu$, where μ is the chemical potential.

B. Results and outlook

In this paper we take the first step towards understanding how the scaling of the AC conductivity survives the effects of temperature and momentum dissipation. The example we analyze is the simplest possible one: the ultraviolet (UV) theory is a conformal field theory[3] (CFT). The holographic theory this is associated with is the four-dimensional anti00de Sitter geometry (AdS_4). The IR theory is also a CFT but dominated by charge density and has scale invariance in time only. It is associated with the two-dimensional anti-de Sitter geometry (AdS_2).

There is a characteristic scale that controls the passage from AdS_4 to AdS_2 (at $T = 0$) and this is the charge density (or its thermodynamic dual, the chemical potential μ). We also add momentum dissipation. This introduces a new characteristic (mass) scale k that competes with the charge density. We have, in total, three scales: μ, T, and k. Therefore this theory depends on two dimensionless ratios, τ and κ that control the importance of temperature and momentum dissipation

$$\tau = 2\pi\frac{T}{\mu}, \quad \kappa \equiv \frac{k}{\mu}. \tag{8}$$

Moreover, we define the following quantity, related to momentum dissipation:

$$\lambda \equiv \sqrt{\frac{k}{2\mu}} = \sqrt{\frac{\kappa}{2}}. \tag{9}$$

The theory at $\tau = \kappa = 0$ has two scaling regimes. In the UV regime the scaling exponent is $m = 0$ [$z = 1$, $\zeta = 0$ in (6)]. It is a well-known result that in a Lorentz-invariant and scal-invariant theory at zero density, in $d = 2$ the conductivity is a (dimensionless) constant. We normalize, without loss of generality this constant to 1. In the IR, $m = 2$ [$z \to \infty$, $d = 2$, $\theta = 0$ in (7)].

We generically find four distinct regimes.

(1) The Drude regime for

$$\frac{\omega}{\mu} \ll \lambda\,.$$

[2]See also [62,63] for a careful analysis of cases where the AC conductivity depends on irrelevant data in the IR.

[3]The UV theory is assumed to be Lorentz invariant. The charge density breaks the Lorentz-invariance. The IR theory has an emergent scale invariance in time only.

TABLE I. Summary of the regimes in the optical conductivity at finite density, temperature and momentum dissipation.

Regime	frequency	Re[σ]
Drude	$\frac{\omega}{\mu} \ll \lambda$	$\frac{\kappa^2}{\kappa^4+12\omega^2/\mu^2}$
Temperature-dominated	$\lambda \ll \frac{\omega}{\mu} \ll \tau$	$\frac{1}{3}\tau^2$
Scaling	$\max\{\tau,\lambda\} \ll \frac{\omega}{\mu} \ll 1$	$\frac{1}{3}(\frac{\omega}{\mu})^2$
UV	$\frac{\omega}{\mu} \gg 1$	1

In this regime momentum dissipation produces a Drude peak.[4]

(2) The temperature-dominated regime

$$\lambda \ll \frac{\omega}{\mu} \ll \tau \ .$$

Here thermal effects dominate the AC conductivity.

(3) The scaling (intermediate) regime

$$\max\{\tau,\lambda\} \ll \frac{\omega}{\mu} \ll 1 \ .$$

In this regime, if it exists, the AC conductivity is showing its ω^2 IR scaling, unmasked. It exists only if $\max\{\tau,\lambda\}$ is sufficiently smaller than 1.

(4) The UV regime

$$\frac{\omega}{\mu} \gg 1 \ .$$

In this regime the AC conductivity is that of the UV theory, i.e., a constant. It has been normalized to 1.

The four regimes along with the real part of the AC conductivity are summarized in the Table I.

We conclude that our expectations are verified in the simple example that has been analyzed here. The next step is a choice of theory with nontrivial scaling exponents that provide a negative value for the AC exponent m, and study similarly the effects of temperature and momentum dissipation on the visibility of scaling of the AC conductivity. Moreover, this mechanism must be implemented in the more complex context of a theory which contains the competition of phases, giving rise to the strange metal phase diagram, along the lines of [64].

The paper is organised as follows, In Sec. II we introduce the holographic model in consideration and discuss its black-hole solution and equilibrium properties. In Sec. III we compute the frequency dependence of the conductivity in three different regimes, the first case corresponds with the momentum conserving zero temperature case. Then, we switch temperature on and study the conditions for scaling conductivities in the IR regime. As a last step we include relaxation of momentum and study all the possibilities in the IR conductivity. We close our analysis with Sec. IV, where our conclusions are presented and where we discuss possible generalizations.

[4]As before, this is despite the fact that there are no quasiparticles in the holographic theory.

II. REISSNER-NÖRDSTROM BLACK-HOLE AND AdS$_2$ IR-SCALING ASYMPTOTICS

We consider a $2+1$ (scale invariant) CFT with a (global) conserved $U(1)$ charge in a flat Minkowski space-time. The conserved charge allows us to consider the theory at finite charge density, a context relevant for addressing many-body problems. Our scale-invariant QFT is not a generic relativistic theory: it is a large-N theory at nearly infinite coupling constant. Here N is the number of colors and unlike other large-N examples used in condensed matter physics, it includes an $SU(N)$ gauge interaction that makes the theory much more complex.

Such large-N gauge theories at strong coupling are known as "holographic," as they are dual to gravitational theories in higher dimensions (typically one-higher dimension) on nontrivial geometric spaces that are asymptotic to anti–de Sitter space. In our example the dual gravitational theory will have $3+1$ dimensions. The $(3+1)$-dimensional spaces that are relevant have always a boundary that has the same geometry as the space on which the QFT lives. In our case the boundary will be flat $(2+1)$-dimensional Minkowski space. The AdS/CFT correspondence and the associated applications to condensed matter problems are treated in several extensive references [41–48].

As a starting point, we introduce the gravitational action for the system in consideration, which consists of a (bulk)[5] gravitational Einstein-Maxwell theory in $3+1$ space-time dimensions, coupled to a set of axion fields[6] responsible for the nonconservation of momentum in the boundary field theory [65–69].

Einstein-Maxwell theory in $3+1$ dimensions is the holographic (bulk) description of the universal sector of a holographic $(2+1)$-dimensional CFT. It contains a metric $g_{\mu\nu}$, dual to the energy-momentum tensor of the CFT, and a gauge field A_μ, dual to the conserved $U(1)$ current. We also introduced a source of momentum dissipation in the theory that is generated by two scalar fields $\phi_{1,2}$ without a potential. Such fields, which we call axions, implement a source of momentum dissipation in the continuum limit.

The action for the bulk theory is

$$S = \frac{1}{16\pi G_N}\int \mathrm{d}^4x\sqrt{-g}\Big(R + \frac{6}{L^2} - \frac{L^2}{4}F_{\mu\nu}F^{\mu\nu} - \frac{1}{2}\sum_{n=1}^{2}\partial_\mu\phi_n\partial^\mu\phi_n\Big), \tag{10}$$

where R is the Ricci scalar of the bulk metric and

$$F_{\mu\nu} = \partial_\mu A_\nu - \partial_\nu A_\mu \tag{11}$$

is the field strength of the bulk gauge field.

The equations of motions are shown in Appendix A. Solutions to the equations of motion which are asymptotically

[5]In this work, by bulk we mean the $(3+1)$-dimensional space where the gravitational theory lives, whereas the boundary is $(2+1)$-dimensional and is the space on which the dual QFT lives.

[6]In this work, we refer to axion fields as scalar bulk fields without a potential.

AdS, and have specific boundary conditions at the AdS boundary, are interpreted as saddle points of the CFT.

The theory in (10) admits a charged black-hole solution of the form

$$ds^2 = \frac{L^2}{r^2}\left(-f(r)dt^2 + dx^2 + dy^2 + \frac{1}{f(r)}dr^2\right), \tag{12}$$

$$A_t = \psi(r), \quad \phi_1 = k\,x, \quad \phi_2 = k\,y\,, \tag{13}$$

where

$$f(r) = 1 + \frac{1}{4}q^2r^4 - \frac{1}{2}k^2r^2 - mr^3\,, \tag{14}$$

$$\psi(r) = \mu - q\,r\,, \tag{15}$$

and q, m are proportional to the charge and energy density of the system, respectively.[7] Here, x, y are Cartesian coordinates in space, t is the time, and r is the holographic coordinate. The boundary of the bulk space is at $r = 0$.

The two scalars have linear solutions that break translational invariance in the spatial directions and therefore provide a source of momentum dissipation. We chose the parameters of that solution so that rotational invariance remains intact (mostly for simplicity). We can generalize this to a solution where momentum dissipation is different along different spatial directions. The regularity condition at the horizon implies that

$$q = \frac{\mu}{r_0}\,, \tag{16}$$

where r_0 is the horizon radius.

At this point, it is important to review the parameters that enter in the solution.[8] First of all, the gravitational action has two-dimensional parameters. One is the bulk Newton's constant G_N and the other is the AdS curvature length L. The dimensionless number is

$$\frac{L^2}{G_N} \sim N^2 \;\gg\; 1, \tag{17}$$

where N^2 is the number of adjoint degrees of freedom of the quantum field theory. Only L enters the solution. The rest of the parameters involve the following.

(1) The mass of the black-hole m, which gives the energy of the canonical ensemble.

(2) The charge q, with dimension of mass^2, that determines the charge density of the dual CFT.

(3) The parameter μ with dimension of mass that determines the chemical potentials of the dual CFT. It is related to the charge density via the relation in (16).

(4) The parameter k, with dimension of mass (or inverse length), that controls the breaking of translation invariance and therefore the rate of momentum dissipation in the system.

(5) The temperature T of the ensemble is fixed and related to the other parameters in a way we shall describe below.

The horizon radius r_0 is related also to other parameters of the solution. To fix the value of r_0 in terms of the physical scaling parameters T, μ, k we need to solve for the condition $f(r_0) = 0$, where r_0 is given by the smallest positive solution[9] of the polynomial in x,

$$1 + \frac{1}{4}q^2x^4 - \frac{1}{2}k^2x^2 - mx^3 = 0\,. \tag{18}$$

For $q \neq 0$, the polynomial (18) always has exactly two positive real roots r_1, r_2. As long as the following inequality is satisfied:

$$108m^2 > k^2(k^4 - 36q^2) + (k^4 + 12q^2)^{3/2}, \tag{19}$$

the other two roots are complex. If (19) is not satisfied, the other two roots are also real, but negative, hence they do not affect us since r is nonnegative in our coordinate system. We can now factorize the blackening factor as follows:

$$f(r) = \left(1-\frac{r}{r_1}\right)\left(1-\frac{r}{r_2}\right)\left(1+\frac{r_1+r_2}{r_1r_2}r+\frac{r_1^2+r_1r_2+r_2^2}{r_1^2r_2^2}r^2\right), \tag{20}$$

where the two positive real roots r_1, r_2 satisfy

$$\frac{1}{2}k^2 + \frac{1}{4}q^2r_1r_2 = \frac{1}{r_2^2} + \frac{1}{r_1r_2} + \frac{1}{r_2^2}\,, \tag{21}$$

$$m = \frac{r_1^3 + r_1^2r_2 + r_1r_2^2 + r_2^3}{r_1^3r_2^3}. \tag{22}$$

Finally we identify $r_0 = \min(r_1, r_2)$ with the black-hole horizon, and $r_\star = \max(r_1, r_2)$ as the interior (Cauchy) horizon[10] characteristic of charged black holes. The Hawking temperature for such a black hole reads

$$T = \frac{1}{4\pi r_0}\left(3 - \frac{1}{2}k^2r_0^2 - \frac{1}{4}q^2r_0^4\right), \tag{23}$$

which can be shown to be positive definite, after using (21) to construct the following relation:

$$\frac{1}{2}k^2r_0^2 + \frac{q^2r_0^4}{4} \leqslant \frac{1}{2}k^2r_0^2 + \frac{q^2r_0^3r_\star}{4} = \frac{r_0^2}{r_\star^2} + \frac{r_0}{r_\star} + 1 \leqslant 3. \tag{24}$$

The inequality is saturated at extremality ($r_0 = r_\star$) where the temperature vanishes. In addition, the black-hole mass can be written as

$$m = \frac{4 - 2r_0^2k^2 + r_0^2\mu^2}{4r_0^3}. \tag{25}$$

Considering we are interested in exploring the low temperature properties of the geometry and the optical conductivity, it is convenient to introduce the scaling (dimensionless) variables

$$\tau = 2\pi\frac{T}{\mu}, \quad \kappa = \frac{k}{\mu}\,. \tag{26}$$

In terms of the dimensionless temperature τ and momentum relaxing parameter κ, the black-hole horizon radius r_0 can be

[7] This black-hole solution is the saddle point that described the ground state of the theory at finite temperature and $U(1)$ charge.

[8] We use units where $c = \hbar = 1$.

[9] Notice that the boundary is sitting at $r = 0$, and the outer horizon corresponds with the smallest positive solution of $f(r_0)$.

[10] Notice that in our coordinates the boundary sits at $r = 0$.

written as

$$\mu r_0 \equiv F(\tau,\kappa) = \frac{6}{\sqrt{6\kappa^2+4\tau^2+3}+2\tau}\,. \tag{27}$$

Therefore, the corresponding thermodynamic quantities, energy density ϵ, entropy density s, and charge density q, take the following form:

$$\begin{aligned}\mu^{-3}\epsilon &= 2F(\tau,\kappa)^{-3}+\frac{1-2\kappa^2}{2}F(\tau,\kappa)^{-1},\\ \mu^{-2}s &= 4\pi F(\tau,\kappa)^{-2},\\ \mu^{-2}q &= F(\tau,\kappa)^{-1}.\end{aligned} \tag{28}$$

IR (near-extremal) AdS_2 geometry

As it is well known [50] that the zero temperature near-horizon geometry of this black hole is $AdS_2\times\mathbb{R}^2$. To make this manifest, we rewrite the blackening factor f as follows

$$\begin{aligned}f(R) = 2\tau F^2\frac{R}{L^2\mu}+\frac{F^3[(\kappa^2+1)F-4\tau]}{2}\frac{R^2}{\mu^2L^4}\\ +\frac{F^4[2\tau-(\kappa^2+2)F]}{3}\frac{R^3}{\mu^3L^6}+\frac{F^6}{4}\frac{R^4}{\mu^4L^8},\end{aligned} \tag{29}$$

with

$$R = \frac{L^2}{r_0^2}(r_0-r), \tag{30}$$

and F the function defined in (27). In terms of the new radial coordinate R, the metric reads

$$\begin{aligned}ds^2 = \frac{L^6}{r_0^2(L^2-r_0R)^2}\left(-f(R)\,dt^2+\frac{r_0^4}{L^4}\frac{dR^2}{f(R)}\right)\\ +\frac{L^6}{r_0^2(L^2-r_0R)^2}d\vec{x}^2\,.\end{aligned} \tag{31}$$

At zero temperature ($\tau=0$) and in the region where $R\ll\mu L^2$, the space-time is approximately $AdS_2\times\mathbb{R}^2$:

$$ds^2 = -\frac{R^2}{L_{IR}^2}dt^2+\frac{L_{IR}^2}{R^2}dR^2+\frac{L^2}{r_0^2}d\vec{x}^2\,, \tag{32}$$

with the AdS_2 radius given by

$$L_{IR}^2 = \frac{1+2\kappa^2}{1+\kappa^2}\frac{L^2}{6}\,. \tag{33}$$

If τ is finite but small, in the region near the horizon

$$\frac{R}{\mu L^2}\ll 1, \tag{34}$$

we obtain an $AdS_2\times\mathbb{R}_2$ black hole

$$ds^2 = -g(R)dt^2+\frac{dR^2}{g(R)}+\frac{L^2}{r_0^2}d\vec{x}^2, \tag{35}$$

where

$$g(R) = \frac{R^2}{L_{IR}^2}\left(1-\frac{(6+8\kappa^2)\tau}{(1+\kappa^2)\sqrt{3+6\kappa^2}}-\frac{2\tau\sqrt{3+6\kappa^2}}{3R(1+\kappa^2)}\right)+\mathcal{O}(\tau^2). \tag{36}$$

In the intermediate region

$$\tau\frac{L_{IR}^2}{L^2}\ll\frac{R}{\mu L^2}\ll 1, \tag{37}$$

we have

$$g(R)\approx\frac{R^2}{L_{IR}^2}\left(1-\tau\frac{2(4\kappa^2+3)}{(1+\kappa^2)\sqrt{3+6\kappa^2}}\right)=\frac{R^2}{L_{IR}'^2}, \tag{38}$$

where we defined

$$L_{IR}'^2 = L_{IR}^2\left(1+\tau\frac{2(4\kappa^2+3)}{(1+\kappa^2)\sqrt{3+6\kappa^2}}+\mathcal{O}(\tau^2)\right). \tag{39}$$

Therefore in the region (37) we still have an $AdS_2\times\mathbb{R}^2$ geometry

$$ds^2 = -\frac{R^2}{L_{IR}'^2}dt^2+\frac{L_{IR}'^2}{R^2}dR^2+\frac{L^2}{r_0^2}d\vec{x}^2, \tag{40}$$

with a modification to the AdS_2 radius stemming from the blackening factor of the AdS_2 black hole.

III. AC CONDUCTIVITY AND ITS CRITICAL IR SCALING

We now study the AC conductivity of our theory, and in particular its scaling form in appropriate frequency ranges.

To understand the conditions under which scaling tails appear in the system, we consider first the zero temperature ($\tau=0$) and momentum conserving case ($\kappa=0$).

To compute the AC conductivity, we introduce perturbations propagating on the extremal ($\tau=0$) Reissner-Nördstrom black-hole solution, and use linear response, following the prescription introduced in [70].

After studying the zero temperature case, we turn-on a small temperature in the system. In the last step, in addition to the temperature, we also include momentum relaxation.

A. IR scaling of the AC conductivity

We begin with vanishing temperature and absence of momentum relaxation. The background is equivalent to the extremal AdS-Reissner-Nördstrom black hole which has no independent dimensionless parameters. The fluctuation equation relevant for the computation of the electrical conductivity reads (see Appendix B for the derivation)

$$fa_x''+f'a_x'+12\left(\frac{w^2}{f}-\rho^2\right)a_x = 0\,, \tag{41}$$

where the frequency is measured in units of chemical potential

$$w = \frac{\omega}{\mu} \tag{42}$$

and

$$f(\rho) = (1-\rho)^2(1+2\rho+3\rho^2),\qquad \rho = r/r_0\,. \tag{43}$$

For the extremal black-hole, the horizon is located at $(\mu r_0)^2=12$. In particular, (41) has an irregular singular point at $\rho=1$, implying a near-horizon behavior given by

$$a_x\sim(1-\rho)^{-4\sqrt{3}/9iw}e^{\frac{iw}{\sqrt{3}(1-\rho)}}. \tag{44}$$

After numerically solving the differential equation with the near-horizon condition (44), the frequency dependence of the

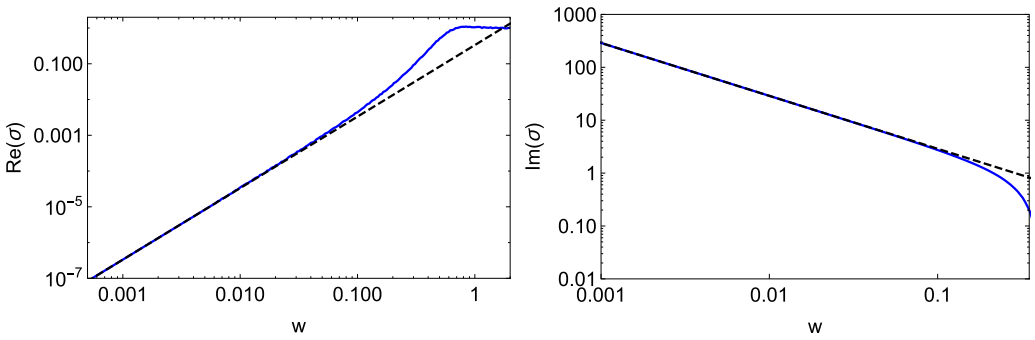

FIG. 2. Frequency dependence of the conductivity at $\tau = \kappa = 0$. The real part (left) shows the scaling behavior $\mathrm{Re}[\sigma] \sim w^2$. On the contrary, the imaginary part (right) shows a $\mathrm{Im}[\sigma] \sim w^{-1}$ divergence, indicating the presence of a $\delta(w)$ in the real part, as required by momentum conservation. The black dashed line corresponds to the fitting $\mathrm{Re}[\sigma] = w^2/3$ and $\mathrm{Im}[\sigma] = 1/(2\sqrt{3}w)$.

conductivity can be computed. The results are shown in Fig. 2. As expected, for $w \ll 1$ the AdS_2 geometry dominates and an IR scaling emerges.

To understand the intuition behind this, we must present some facts in the holographic (gravitational) description of strongly coupled theories. First, the bulk space where gravity lives has an extra dimension that plays roughly the role of the renormalization group scale of the dual quantum field theory. Near the boundary, the region corresponds to the UV regime. As we move towards the interior of the geometry, we are moving towards the IR limit of the dual quantum field theory. The ultimate interior is bounded by the horizon of the bulk black hole. Therefore, the region near the horizon is controlling the IR physics of the dual quantum field theory. In our example, this region has the AdS_2 geometry and is therefore an AdS_2 black hole.

By fitting the numerical data, the conductivity can be written as

$$\sigma(w) = \frac{1}{3}w^2 + \frac{1}{2\sqrt{3}}\left(\delta(w) + \frac{i}{w}\right) + \cdots, \qquad w \to 0, \tag{45}$$

in agreement with the general scaling exponents derived in [60]. We also included the δ-function in the real part, which is there due to the $1/w$ pole in the imaginary part. To finish the numerical analysis of the conductivity, we proceed to plot the absolute value $|\sigma|$ and the argument $\arg\sigma$ as shown in Fig. 3. In the left plot, the $1/w$ pole of the imaginary part dominates over the w^2 scaling of the real part. In the right plot, the argument takes the value $\arg\sigma = \pi/2$ in the IR, consistent with

$$\arg\sigma \approx \arctan\frac{\sqrt{3}}{2w^3} \approx \frac{\pi}{2} - \frac{2w^3}{\sqrt{3}} + \cdots. \tag{46}$$

On the contrary in the UV region ($w \gg 1$) the behavior is determined by the asymptotic AdS_4 region

$$\sigma(w) = 1, \quad \mathrm{Arg}(\sigma) = 0. \tag{47}$$

B. Temperature versus critical IR scaling of the AC conductivity

Having understood the zero temperature conductivity, we now introduce a nonvanishing τ, while keeping $\kappa = 0$. In this case τ is the only dimensionless parameter. Therefore, the conductivity depends parametrically only on the dimensionless temperature τ.

The equation of motion for the fluctuating gauge field reads (see Appendix B)

$$f a_x'' + f' a_x' + F^2\left(\frac{w^2}{f} - z^2\right)a_x = 0\,, \tag{48}$$

with the blackening factor

$$f(\rho) = 1 - \rho^3 + \frac{1}{4}F^2\rho^3(\rho - 1). \tag{49}$$

The IR conductivity can be studied analytically for $w \ll 1$. For concreteness we show here the result and refer the reader

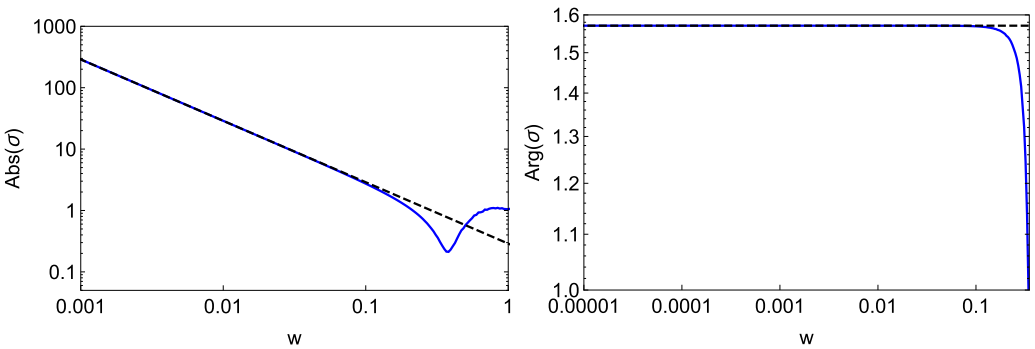

FIG. 3. Absolute value (left) and argument of the conductivity (right) at zero temperature and zero momentum breaking parameter ($\tau = \kappa = 0$). The dashed line shows a fitting with $|\sigma| = \frac{1}{2\sqrt{3}w}$ and $\arg[\sigma] = \frac{\pi}{2}$, respectively.

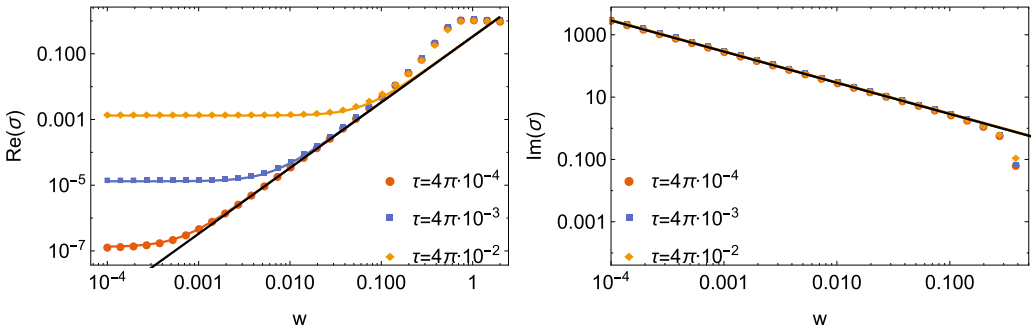

FIG. 4. Finite temperature conductivity at zero momentum relaxation parameter ($\kappa = 0$). In the left plot we show the real part for several values of the temperature τ. The $\delta(w)$ in the real part is not drawn. In the right plot the imaginary part is shown. The dots represent numerical data, while the continuous lines are given by (53). The black lines correspond to $\mathrm{Re}[\sigma] = \frac{1}{3}w^2$ and $\mathrm{Im}[\sigma] = 1/(2\sqrt{3}w)$.

to Appendix B for the details of the computation. In the regime $w \ll 1$, the conductivity reads

$$\sigma(w) \approx \sigma_Q + D\left(\delta(w) + \frac{i}{w}\right), \tag{50}$$

where

$$\sigma_Q = \left(\frac{12 - F^2}{3(4 + F^2)}\right)^2, \quad D = \frac{4F}{3(4 + F^2)}. \tag{51}$$

In particular, in the regime of interest ($\tau \ll 1$), the low-frequency conductivity takes the simple form

$$\sigma(w) \approx \frac{1}{3}\tau^2 + \frac{i}{2\sqrt{3}w}. \tag{52}$$

Having understood the small frequency analysis, we proceed to solve numerically (48), and show the results in Figs. 4 and 5. In the left plot, we observe how temperature introduces the constant offset (σ_Q) to the real part. We shall refer to the regime where this constant value dominates as the temperature-dominated regime. If the condition $\tau \ll w \ll 1$ is satisfied, we notice the emergence of the AdS_2 scaling $\sim w^2$. For high-enough temperatures, the temperature-dominated regime "covers" the scaling regime and, thus, the latter is not visible. Given this behavior, we propose the following form for the low-frequency conductivity:

$$\sigma(w) \approx \sigma_Q + D\left(\delta(w) + i\frac{1}{w}\right) + \frac{1}{3}w^2, \tag{53}$$

which is shown as continuous lines in Figs. 4 and 5.

In addition, we plot the absolute value and argument of the conductivity for different temperatures in Fig. 5. In this case, as it also happens at zero temperature, the $1/w$ imaginary part of the conductivity always dominates in the IR part of the absolute value of the conductivity. This is easy to see from (53). For the w^2 term to "win" over D/w we need $D \ll w^3$. However, for $\tau \ll 1$, we have $D \approx 0.29 \gg w^3$. Finally, the argument has a similar behavior to the zero-temperature case at small frequencies. For $\tau \ll 1$ it reads

$$\arg(\sigma) = \frac{\pi}{2} - \frac{2}{\sqrt{3}}w(w^2 + \tau^2) + \cdots. \tag{54}$$

C. Momentum dissipation versus IR scaling of the AC conductivity

The last case to be considered is the general case of finite temperature and momentum relaxing parameter. The system is controlled by the two dimensionless parameters τ, κ. For the present case, the gauge field couples to the scalar and metric sector (see Appendix B), therefore we need to solve the system of equations

$$\frac{wF^2}{\rho^2 f}(w\chi - i\kappa h_t^x) + (\rho^{-2} f \chi')' = 0, \tag{55}$$

$$-\frac{i\rho^2 F^2 w}{f}a_x + \frac{iw}{f}h_t^{x'} - \kappa\chi' = 0, \tag{56}$$

$$-h_t^{x'} + \frac{w^2 F^2 a_x}{f} + (f a_x')' = 0, \tag{57}$$

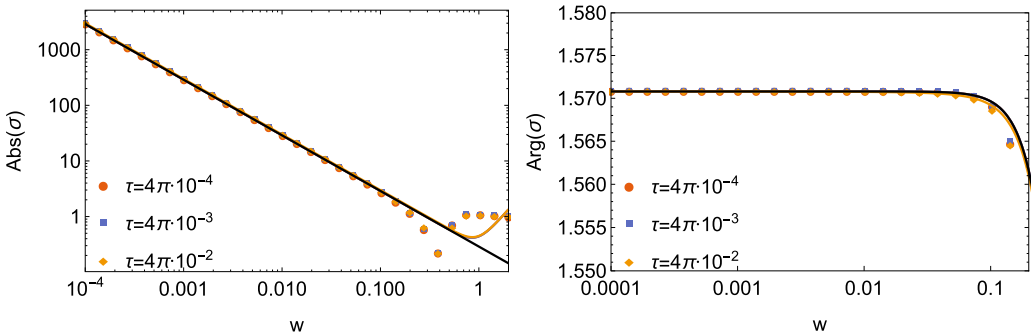

FIG. 5. The absolute value and argument of the conductivity at $\kappa = 0$ and at various value of τ. The dots show the numerical data, while the continuous lines are given by (53). The black line shows a fitting with the zero temperature result $|\sigma| = \frac{1}{2\sqrt{3}w}$ and $\arg[\sigma] = \frac{\pi}{2} - \frac{2}{\sqrt{3}}w^3$.

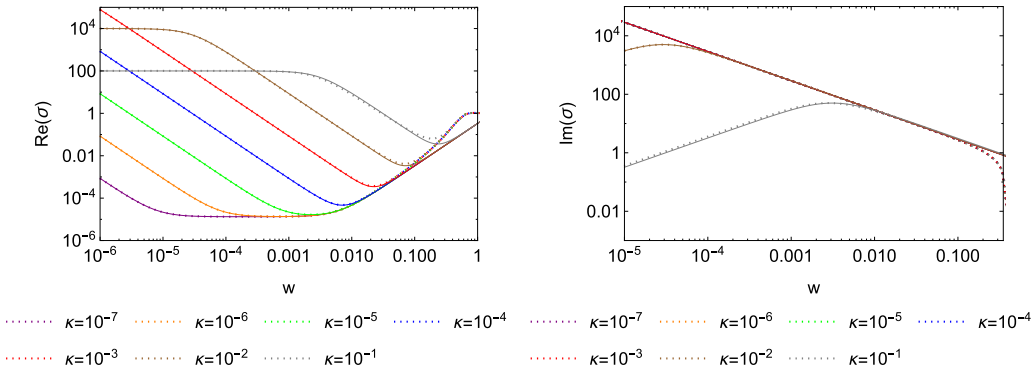

FIG. 6. The real and imaginary parts of the conductivity at $\tau = 2\pi \times 10^{-3}$ and for various values of κ. The dots show the numerical data, while the continuous lines are given by (62). Note that the peaks that appear in the real part as $w \to 0$ are not visible in this plot for most values of κ. As we further decrease the frequency, the lines cross and the peaks appear in reverse order.

where the blackening factor takes the form

$$f(\rho) = (1-\rho)\left(1+\rho+\rho^2-\frac{1}{2}\kappa^2F^2\rho^2-\frac{1}{4}F^2\rho^3\right). \quad (58)$$

In Appendix B we solve the fluctuation equation perturbatively for $wF \ll 1$ and $\kappa F \ll 1$, where F was defined in (27). The conductivity in this limit is given by

$$\sigma(w) \approx \frac{D+\mathcal{O}(wF,\kappa^2F^2)}{\Gamma - iw + O(w^2F^2, w\kappa^2F^3, \kappa^4F^4)} + \sigma_Q + \mathcal{O}(wF,\kappa^2F^2), \quad (59)$$

where

$$\sigma_Q = \left(\frac{12-F^2}{3(4+F^2)}\right)^2, \quad D = \frac{4F}{3(4+F^2)}, \quad \Gamma = \kappa^2 D\,. \quad (60)$$

Actually, in the $\kappa \ll 1$ and $\tau \ll 1$ limit, the leading behavior of the coefficients is given by

$$D = \frac{1}{2\sqrt{3}}, \quad \Gamma = \frac{\kappa^2}{2\sqrt{3}}, \quad \sigma_Q = \frac{\tau^2}{3}. \quad (61)$$

Since for $\kappa \ll 1, \tau \ll 1$ we have $F^{-1} \simeq 0.3$, the approximation is valid in the region of interest ($w \ll 1$).

The term of order κ^2 in the numerator of (59) was calculated in [71] and is included in (62). This term is important to obtain the exact DC conductivity in the $w \to 0$ limit, however, it is negligible in the parameter range we are interested in.

After the approximate analytic analysis, we solve numerically for the conductivity, and show the results in Figs. 6 and 7. For the computation of the conductivity we fixed $\tau = 2\pi \times 10^{-3}$, and analyze the transport coefficient for several values of κ. To fit the numerical data, in addition to the analytically computed conductivity (59) we add to the real part the power law $1/3w^2$, and show the function as continuous lines in Figs. 6 and 7. In particular, we observe that for $\kappa = 0.1$ the fit is not very good. This is because we are approaching the boundary of the validity region of the formula (59) ($\kappa \ll F^{-1} \sim 0.3$).

We observe that the formula

$$\sigma(w) \approx \frac{D+\Gamma(1-\sigma_Q)}{\Gamma - iw} + \sigma_Q + \frac{1}{3}w^2 \quad (62)$$

approximates well the numerical data as long as $\kappa \ll F^{-1} \sim 0.3$.

We study now the conditions for the scaling of the AC conductivity to be visible. To do so, we write the real part for $\tau \ll 1, \kappa \ll 1, w \ll 1$ as follows:

$$\mathrm{Re}[\sigma] \approx \underbrace{\frac{\kappa^2}{\kappa^4+12w^2}}_{\text{Drude}} + \underbrace{\frac{\tau^2}{3}}_{\text{temperature}} + \underbrace{\frac{w^2}{3}}_{\text{scaling}}. \quad (63)$$

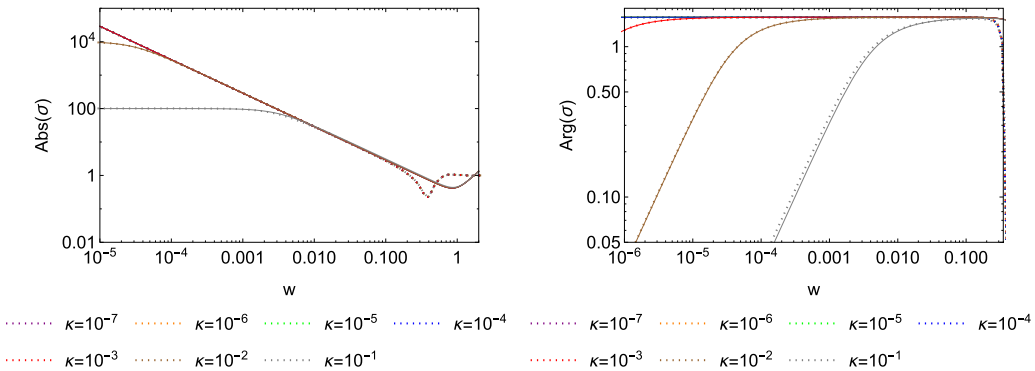

FIG. 7. The absolute value and argument of the conductivity at $\tau = 2\pi \times 10^{-3}$ and for various values of κ. The dots show the numerical data, while the continuous lines are given by (62).

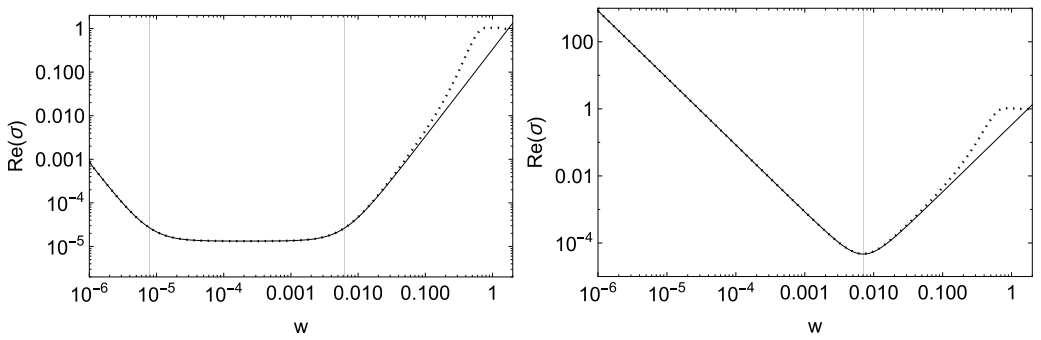

FIG. 8. Real part of the conductivity as a function of the frequency at $\tau = 2\pi \times 10^{-3}$. Left plot ($\kappa = 10^{-7}$) shows the conductivity for the case in which $\lambda \ll \tau \ll 1$. The Drude peak turns into the "flat" temperature-dominated behavior, which gives its turn to the scaling behavior $\sim w^2$, before reaching the UV at $w > 1$. The vertical lines correspond to $\frac{\kappa}{(2\tau)}$ and τ from left to right. On the contrary the right plot ($\kappa = 10^{-4}$) corresponds to regime $\tau \ll \lambda \ll 1$. The Drude peak shows a transitions directly to the $\sim w^2$ scaling behavior. The dashes show the numerical data, while the continuous line is given by (63). The vertical line corresponds to $\lambda = \sqrt{\frac{\kappa}{2}}$.

We observe a "Drude peak" as long as $\kappa \neq 0$, which dominates for small-enough frequency. As w increases, either the scaling or temperature terms starts to dominate. Therefore we divide the analysis in the following two cases.[11]

(1) Temperature dominated $\lambda \ll \tau \ll 1$: In this case, as we turn the frequency on, the temperature term in (63) is the first one to start dominating over the Drude term at frequencies of order $w \sim \kappa/(2\tau)$. Then, as we keep increasing w, the scaling term becomes dominant. The temperature-dominated behavior appears for frequencies $\kappa/(2\tau) \ll w \ll \tau$, while the scaling in the conductivity is visible for $\tau \ll w \ll 1$. In particular, in the left plot of Fig. 8 we tuned the parameters to sit within this regime ($\kappa = 10^{-7}$, $\tau = 2\pi \times 10^{-3}$) and we notice the three well-defined regions, Drude, temperature-dominated, and scaling, respectively, in consistency with this classification.

(2) Drude dominated $\tau \ll \lambda \ll 1$: This case is characterized by the "Drude peak" covering the flat region, but not the scaling regime. In fact, when $w \sim \lambda$ the scaling contribution in the conductivity starts dominating as can be seen in the right plot of Fig. 8.

The previous analysis suggests that as long as $\tau \ll 1$ and $\lambda \ll 1$, the critical scaling will be visible within the window

$$\max\{\tau, \lambda\} \ll w \ll 1. \tag{64}$$

Finally, to extract the behavior of the absolute value and argument of the conductivity we proceed to write the full conductivity as follows:

$$\sigma = \frac{D\Gamma}{\Gamma^2 + w^2} + \sigma_Q + \frac{1}{3}w^2 + i\frac{Dw}{\Gamma^2 + w^2} + \cdots . \tag{65}$$

However, in the region given by (64) where the scaling is visible, the conductivity takes the approximate form

$$\sigma \approx \frac{1}{3}w^2 + i\frac{D}{w} + \cdots , \tag{66}$$

which automatically implies that the imaginary part will be dominant in the absolute value of the conductivity because $D \approx \frac{1}{2\sqrt{3}}$ and the frequency is $w \ll 0.1$. On the other hand, the argument at zero frequency vanishes as

$$\mathrm{Arg}[\sigma] \approx \arctan\frac{2\sqrt{3}w}{\kappa^2}, \tag{67}$$

and approaches $\mathrm{Arg}[\sigma] \approx \pi/2$ when the frequency is within the values given by the interval (64).

IV. CONCLUSION

There are several strange metals that exhibit special scaling laws in their AC conductivities as functions of frequency [31–33]. There are also other systems that are strongly coupled and exhibit criticality, like fermions at unitarity [72] (see [73] for a recent review). Such systems are nonrelativistic and scale invariant with Lifshitz exponent $z = 2$ and extended Schrödinger symmetry, that is, the analog of conformal symmetry in relativistic systems.[12] They have been experimentally realized in terms of cold atomic gases [74]. Scaling AC spin conductivities were calculated and observed in such systems, [75]. The behavior is similar to the cuprates, but the scaling exponent is different. A second class of examples encompasses Dirac materials. Their zero density phase can be seen as a semimetal quantum critical point, connecting metallic electron and hole phases. Strictly speaking, these systems are not scale invariant since long-range interactions break the symmetry, introducing logarithmic corrections to the power law in their corresponding conductivities. In $2+1$ dimensions, scale invariance requires a constant conductivity, whereas in $3+1$ the conductivity should grow linearly. In fact, such power laws have been predicted in [76], and experimentally seen in graphene and Dirac/Weyl semimetals [77].[13]

The two conditions, strong coupling and criticality, are combined in strongly coupled holographic theories. Such theories were shown to exhibit an AC conductivity that is

[11]We only study the cases where the scaling survives. If either the temperature or the momentum relaxing parameter are large enough, the critical scaling power law is no longer visible in the AC conductivity.

[12]There are holographic (strongly coupled) theories exhibiting Schrödinger symmetry [78].

[13]For a holographic description, see also [79].

a scaling function of the frequency ω in the IR regime [35,59,60].

We embarked here in a study of how nonzero temperature and momentum dissipation affect the visibility of scaling in the AC conductivity. In this paper, we studied perhaps the simplest holographic theory at finite density, a $2+1$ dimensional (relativistic) CFT.

Such a theory is known to exhibit an unexpected one-dimensional scale invariance in the IR at finite density [50]. This invariance is intimately tied to the appearance of the AdS_2 geometry in the near-horizon region of the near-extremal AdS-Reissner-Nördstrom black hole.

We studied the effects that temperature and relaxation of momentum have on near-extremal black-holes with AdS_2 geometry. We showed, that as long as the condition

$$\max\{\tau, \lambda\} \ll w \ll 1, \tag{68}$$

is satisfied, the real part of the electrical conductivity will show the critical scaling behavior determined by the AdS_2 near-horizon geometry. In (68), τ is the dimensionless temperature $\lambda = \sqrt{\kappa/2}$, where κ is the dimensionless momentum dissipation coefficient and w is the rescaled frequency, as defined in (26), (9), and (42). The imaginary part of the conductivity is generically dominated by the Drude peak in this example.

From this example we conclude that the visibility of the mid-range scaling of the AC conductivity depends crucially on the detailed scales of the material that determine whether the temperature and momentum dissipation mask the scaling region. We found the conditions for this to happen. This may explain why in some cuprates such a scaling is visible experimentally while in others it is not. It would be interesting to combine independent experimental data on quantifying momentum dissipation in various cuprate materials and correlate this with the visibility of scaling in the AC conductivity.

The next step is to investigate more complex holographic systems that have a closer resemblance to strange metals, where $\sigma(\omega) \sim \omega^{-a}$ with $0 < a < 1$ [60]. As was shown in [60], the exponent a is bounded by the unitarity limit $a = 1$, while the contribution of the Drude peak provides a $1/\omega$ tail as $\omega \to 0$. Therefore, at higher values of ω we expect the critical conductivity to dominate over the Drude peak. Moreover, as shown in [60], the phase of the complex AC critical conductivity is constant and coincides with that suggested by the real part ω^{-a}. Therefore, we expect that if and when this part dominates, it will have the form seen in experiments.

ACKNOWLEDGMENTS

We thank B. Goutéraux, N. Hussey, A. Mackenzie, C. Panagopoulos, K. Schalm, D. Son, D. Van der Marel, and J. Zaanen for useful discussions. We also thank B. Goutéraux and J. Zaanen for critical comments on the manuscript. Last but not least, we would like to thank the referees for their suggestions and corrections. This work was supported in part, by the European Research Council via the Advanced ERC Grant SM-grav, No. 669288, and the Deutsche Forschungsgemeinschaft (DFG, German Research Foundation) under Germany's Excellence Strategy through Würzburg-Dresden Cluster of Excellence on Complexity and Topology in Quantum Matter - ct.qmat (EXC 2147, Project No. 390858490). F. P-B acknowledges the Quantum Matter Academy of ct.qmat for support.

APPENDIX A: EQUATIONS OF MOTION

Taking variations of the action respect to the metric, gauge, and scalar fields we obtain the following set of equations of motion:

$$R_{\mu\nu} = -\frac{3}{L^2} g_{\mu\nu} + \frac{1}{2}(\partial_\mu\phi_1\partial_\nu\phi_1 + \partial_\mu\phi_2\partial_\nu\phi_2) + \frac{1}{2}\left[F_\mu{}^\rho F_{\nu\rho} - \frac{g_{\mu\nu}}{4}F^2\right], \tag{A1a}$$

$$\nabla_\mu F^{\mu\nu} = 0, \tag{A1b}$$

$$\nabla_\mu\nabla^\mu\phi_i = 0, \quad i = 1, 2, \tag{A1c}$$

where the covariant derivatives are defined with the Christoffel connection.

We consider static, rotationally symmetric (in the x-y plane) solutions, with translational symmetry broken only by the axion fields

$$\begin{aligned} ds^2 &= -D(r)dt^2 + B(r)dr^2 + C(r)dx_i dx^i, \\ \phi_i &= kx_i, \quad A_\mu = [A_t(r), 0, 0, 0], \end{aligned} \tag{A2}$$

where $i = x, y$ above. Substituting the ansatz (A2) into (A1) we obtain the following set of independent equations (the scalar equation of motion are identically satisfied):

$$\frac{6}{L^2}B + L^2\frac{A_t'^2}{2D} + \frac{B'D'}{2BD} - \frac{C'D'}{CD} + \frac{D'^2}{2D^2} - \frac{D''}{D} = 0 \tag{A3a}$$

$$-2\frac{C''}{C'} + \frac{C'}{C} + \frac{B'}{B} + \frac{D'}{D} = 0, \tag{A3b}$$

$$k^2\frac{B}{C} - \frac{6}{L^2}B + \frac{L^2A_t'^2}{2D} - \frac{B'C'}{2BC} + \frac{C'D'}{2CD} + \frac{C''}{C} = 0, \tag{A3c}$$

$$\left(\frac{CA_t'}{\sqrt{BD}}\right)' = 0. \tag{A3d}$$

We are interested in asymptotically AdS_4 solutions. Under this requirement, the regular solution of (A3) is given by

$$ds^2 = \frac{L^2}{r^2}\left(-f(r)dt^2 + dx^2 + dy^2 + \frac{1}{f(r)}dr^2\right), \tag{A4}$$

$$A_t = \psi(r), \quad \phi_1 = k\,x, \quad \phi_2 = k\,y\,, \tag{A5}$$

where

$$f(r) = 1 + \frac{1}{4}q^2r^4 - \frac{1}{2}k^2r^2 - mr^3\,, \tag{A6}$$

$$\psi(r) = \mu - q\,r\,, \tag{A7}$$

and q, m are proportional to the charge and energy density of the system, respectively

APPENDIX B: DERIVATION AND ANALYSIS OF THE AC CONDUCTIVITY

In this Appendix, we derive the equations that determine the AC conductivity in our theory. This is done by deriving the equations of the linear fluctuations around the solutions that perturb the charge density, solving them and then extracting

the IR limit of the current-current correlator from the near-boundary expansion.

To study the linear response of the system, we introduce the relevant fluctuating fields [80]

$$\delta A_x = a_x(r)e^{-i\omega t}, \quad \delta g_t^x = \frac{r^2}{L^2}h_t^x(r)e^{-i\omega t}, \quad \delta\phi_1 = \chi(r)e^{-i\omega t}. \tag{B1}$$

The linearized equations of motion, for the fluctuations, stemming from the equations (A1), are

$$\frac{\omega}{r^2 f(r)}[\omega\chi(r) - ikh_t^x(r)] + [r^{-2}f(r)\chi'(r)]' = 0, \tag{B2a}$$

$$\frac{ir^2\omega A_t'(r)}{f(r)}a_x(r) + \frac{i\omega}{f(r)}h_t^{x'}(r) - k\chi'(r) = 0, \tag{B2b}$$

$$A_t'(r)h_t^{x'}(r) + \frac{\omega^2 a_x(r)}{f(r)} + [f(r)a_x'(r)]' = 0. \tag{B2c}$$

1. Small frequency solution without momentum dissipation

Starting from (B2), we set $k = 0$ and define the following dimensionless variables:

$$\tau = 2\pi\frac{T}{\mu}, \quad w = \frac{\omega}{\mu}. \tag{B3}$$

As we write all physical quantities in units of the chemical potential, for simplicity we will set $\mu = 1$ from now on and for the rest of this section. Equations (B2) can be decoupled to obtain a single equation that governs the fluctuation of the gauge field

$$fa_x'' + f'a_x' + r_0^2\left(\frac{w^2}{f} - \rho^2\right)a_x = 0, \tag{B4}$$

where we are using the rescaled radial coordinate

$$\rho = \frac{r}{r_0}, \tag{B5}$$

and the blackening factor is

$$f(\rho) = (1-\rho)\left(1 + \rho + \rho^2 - \frac{1}{4}r_0^2\rho^3\right). \tag{B6}$$

We now change variables by transforming a_x as follows:

$$a_x = g(\rho)Y(\rho), \quad g(\rho) = 1 - \frac{4r_0^2}{12 + 3r_0^2}\rho \tag{B7}$$

to obtain

$$(fg^2Y')' + r_0^2\frac{w^2}{f}g^2Y = 0. \tag{B8}$$

We now set

$$Y = f(\rho)^{iwr_0/f'(1)}X(\rho), \tag{B9}$$

to remove the leading behavior at the horizon and obtain an equation for $X(\rho)$

$$X'' + \left[\left(1 + \frac{iw}{\tau}\right)\frac{f'}{f} + \frac{2g'}{g}\right]X' + \left(r_0^2\frac{w^2}{f^2} - \frac{w^2f'^2}{4\tau^2f^2} + \frac{iwf'g'}{\tau fg} + \frac{iwf''}{2\tau f}\right)X = 0. \tag{B10}$$

Once the solution for $X(\rho)$ is found, then the conductivity is obtained from the near-boundary behavior, and is given by

$$\sigma(w) = -\frac{i}{wr_0}\left(g'(0) + \frac{X'(0)}{X(0)}\right). \tag{B11}$$

We can find a perturbative solution in the IR by expanding X for small w as follows:

$$X(\rho) = X_0(\rho) + wX_1(\rho) + w^2X_2(\rho) + w^3X_3(\rho) + \cdots. \tag{B12}$$

The equation at each order in w is

$$(fg^2X_n')' = -i\left(g^2X_{n-1}^2f'\right)'/X_{n-1} - g^2X_{n-2}\left[(4\pi\tau)^2r_0^2 - f'^2\right]/f, \tag{B13}$$

with the first two given by

$$\left(fg^2X_0'\right)' = 0, \tag{B14}$$

$$\left(fg^2X_1'\right)' = -i\left(g^2X_0^2f'\right)'/X_0. \tag{B15}$$

We define the following function:

$$H_n = \int_1^\rho \left\{-i\left(g^2X_n^2f'\right)'/X_n - g^2X_{n-1}\left[(2\tau)^2r_0^2 - f'^2\right]/f\right\}d\rho. \tag{B16}$$

Then the solution for X_n can be found recursively by

$$X_n = \int_0^\rho \frac{H_{n-1}}{g^2f}\,d\rho. \tag{B17}$$

The solution for X_0 which is regular at the horizon is just a constant $X_0 = c$. Then X_1 is

$$X_1(\rho) = -ic\int_0^\rho \frac{2\tau g(1)^2 + g(\rho')^2f'(\rho')}{f(\rho')g(\rho')^2}\,d\rho'. \tag{B18}$$

To first order in w, the conductivity is given by

$$\sigma(\omega) = -i\frac{g'(0)}{r_0w} + g(1)^2 + \mathcal{O}(w). \tag{B19}$$

The real part reads

$$\mathrm{Re}[\sigma(\omega)] = (2\tau)^2\left(\frac{2(\sqrt{(2\tau)^2+3} - 2\tau)}{3\left(4 + 2(2\tau)^2 - 4\tau\sqrt{(2\tau)^2+3}\right)}\right)^2 + \mathcal{O}(w^2). \tag{B20}$$

2. Small frequency behavior with weak momentum dissipation

Starting with the system (B2) we define the dimensionless variables

$$\tilde\omega = \omega r_0, \quad \tilde k = kr_0, \quad \tilde q = -qr_0^2, \tag{B21}$$

the radial coordinate

$$\rho = \frac{r}{r_0}, \tag{B22}$$

and rescaling $a_x(r) \to a_x(r)/r_0$ to make it dimensionless, we obtain

$$f(fa_x')' + \tilde q f h_t^{\prime x} + \tilde\omega^2 a_x = 0, \tag{B23a}$$

$$\rho^2 f(f\rho^{-2}\chi')' + \tilde\omega^2\chi - i\tilde\omega\tilde k h_t^x = 0, \tag{B23b}$$

$$i\tilde\omega h_t^{\prime x} - \tilde k f\chi' + i\tilde q\tilde\omega\rho^2 a_x = 0, \tag{B23c}$$

where

$$f(\rho)=(1-\rho)\left(1+\rho+\rho^2-\frac{1}{2}\kappa^2 r_0^2\rho^2-\frac{1}{4}r_0^2\rho^3\right). \quad \text{(B24)}$$

To decouple (B23b), we define the following functions [81]:

$$\phi_\pm=\frac{h_t'^x}{\rho^2}+\tilde{q}a_x+\frac{C_\pm}{\rho}a_x, \quad \text{(B25)}$$

where

$$C_\pm=\frac{6\tilde{k}^2-3\tilde{q}^2-12}{8\tilde{q}}\pm\frac{\sqrt{64\tilde{k}^2\tilde{q}^2+(12-6\tilde{k}^2+3\tilde{q}^2)^2}}{8\tilde{q}}. \quad \text{(B26)}$$

We obtain a decoupled system for $\phi_\pm$

$$(\rho^2 f\phi_\pm')'+\left(\frac{\rho^2\omega^2}{f}+\lambda_\pm\rho\right)\phi_\pm=0, \quad \text{(B27)}$$

where

$$\lambda_+=\frac{C_+f'+\rho(C_-+\tilde{q}\rho)(\tilde{k}^2-C_+\tilde{q}\rho)}{C_+-C_-}, \quad \text{(B28)}$$

$$\lambda_-=\frac{-C_-f'-\rho(C_++\tilde{q}\rho)(\tilde{k}^2-C_-\tilde{q}\rho)}{C_+-C_-}. \quad \text{(B29)}$$

To first nontrivial order in $\tilde{k}$ we have

$$\lambda_+=\tilde{k}^2\left(\frac{\rho(-12-3\tilde{q}^2+4\rho\tilde{q}^2)}{12+3\tilde{q}^2}\right)+\mathcal{O}(\tilde{k}^4), \quad \text{(B30)}$$

$$\lambda_-=-\frac{3}{4}\rho^2(4+\tilde{q}^2)+\tilde{k}^2\left(\frac{\rho[-24-6\tilde{q}^2+(36+\tilde{q}^2)\rho]}{24+6\tilde{q}^2}\right)+\mathcal{O}(\tilde{k}^4). \quad \text{(B31)}$$

We also write f as follows:

$$f(\rho)=f_0(\rho)+\tilde{k}^2 f_1(\rho), \quad \text{(B32)}$$

where

$$f_0(\rho)=(1-\rho)\left(1+\rho+\rho^2-\frac{1}{4}\tilde{q}^2\rho^3\right),$$

$$f_1(\rho)=-\frac{1}{2}\rho^2(1-\rho). \quad \text{(B33)}$$

(1) We start from the equation for ϕ_+ (B25). Using

$$\phi_+=\psi f^{\frac{i\omega}{f'(1)}} \quad \text{(B34)}$$

removes the leading behavior at the horizon. Now ψ must be regular at the horizon.

We expand ψ for small $\tilde{\omega},\tilde{k}$ as follows:

$$\psi=\psi_0+\tilde{\omega}\psi_1+\tilde{k}^2\psi_2+\mathcal{O}(\tilde{\omega}^2,\tilde{k}^4,\tilde{\omega}\tilde{k}^2). \quad \text{(B35)}$$

The equation for ψ_0 is

$$\rho^2 f_0\psi_0'=c_0 \quad \text{(B36)}$$

for which regularity at the horizon implies $c_0=0$, hence ψ_0 is constant. Using this fact we obtain the following equations for ψ_1,ψ_2:

$$(\rho^2 f_0\psi_1')'+\frac{i\psi_0}{f_0'(1)}(\rho^2 f_0')'=0, \quad \text{(B37a)}$$

$$(\rho^2 f_0\psi_2')'+\rho\psi_0 B_1=0,\quad B_1=\frac{\rho(-12-3\tilde{q}^2+4\rho\tilde{q}^2)}{12+3\tilde{q}^2}. \quad \text{(B37b)}$$

From (B37a) we find

$$\psi_1=i\psi_0\int_1^\rho\frac{1}{f_0}\left(\frac{1}{\rho^2}-\frac{f_0'}{f_0'(1)}\right)d\rho\equiv i\psi_0 P_1(\rho). \quad \text{(B38)}$$

From (B37b) we find

$$\psi_2=-\psi_0 P_2(\rho),\quad P_2(\rho)=\frac{4(\rho-1)}{(12+3\tilde{q}^2)\rho}. \quad \text{(B39)}$$

(2) Now we find a perturbative solution for ϕ_-. We first use the transformation

$$\phi_-=gY \quad \text{(B40)}$$

with

$$g=\frac{1}{\rho}-\frac{4\tilde{q}^2}{3(4+\tilde{q}^2)} \quad \text{(B41)}$$

so that the coefficient of Y vanishes at the limit $\tilde{\omega}\to 0,\tilde{k}\to 0$. We use

$$Y=Xf^{\frac{i\omega}{f'(1)}} \quad \text{(B42)}$$

to remove the leading behavior at the horizon. We require that X is regular at the horizon and expand it as follows:

$$X=X_0+\tilde{\omega}X_1+\tilde{k}^2X_2+\mathcal{O}(\tilde{\omega}^2,\tilde{k}^4,\tilde{\omega}\tilde{k}^2). \quad \text{(B43)}$$

For X_0 we find

$$\rho^2 f_0 g^2 X_0'=c, \quad \text{(B44)}$$

which, by regularity at the horizon, implies that X_0 is constant. Using this fact we obtain the following equations:

$$(\rho^2 f_0 g^2 X_1')'+\frac{iX_0}{f_0'(1)}(\rho^2 f_0' g^2)'=0, \quad \text{(B45a)}$$

$$(\rho^2 f_0 g^2 X_2')'+\rho X_0 B_2=0, \quad \text{(B45b)}$$

$$B_2=\frac{2\rho\tilde{q}^2(36+\tilde{q}^2)[\tilde{q}^2(4\rho-3)-12]}{27(4+\tilde{q}^2)^3}. \quad \text{(B45c)}$$

From (B45a) we obtain

$$X_1=iX_0\int_0^\rho\left(\frac{g(1)^2}{\rho^2 f_0 g^2}-\frac{f_0'}{f_0 f_0'(1)}\right)\equiv iX_0 Q_1(\rho). \quad \text{(B46)}$$

From (B45c) we find

$$X_2=-X_0Q_2(\rho),\quad Q_2(\rho)=\frac{8\tilde{q}^2(36+\tilde{q}^2)}{3(4+\tilde{q}^2)[-12+\tilde{q}^2(-3+4\rho)]^2}. \quad \text{(B47)}$$

(3) We now need to fix the integration constants X_0,ψ_0 in terms of the boundary values

$$a_x^{(0)}=a_x(0),\quad \chi^{(0)}=\chi(0),\quad h_t^{x(0)}=h_t^x(0). \quad \text{(B48)}$$

The system (B23) implies the equation

$$f\rho^2(\rho^{-2}h_t'^x + \tilde{q}a_x)' - \tilde{k}^2 h_t^x - i\tilde{k}\tilde{\omega}\chi = 0. \tag{B49}$$

Using (B25) and (B49) we find

$$f(\rho^2\phi_\pm' - C_\pm a_x'\rho + C_\pm a_x) = \tilde{k}^2 h_t^x + i\tilde{k}\tilde{\omega}\chi. \tag{B50}$$

Near the boundary we obtain

$$\lim_{\rho\to 0}(\rho^2\phi_\pm') = -C_\pm a_x^{(0)} + \tilde{k}^2 h_t^{x(0)} + i\tilde{k}\tilde{\omega}\chi^{(0)}. \tag{B51}$$

The expansion of $\phi_\pm$ near the boundary is[14]

$$\phi_\pm = -\frac{W_\pm}{\rho} + D_\pm + \cdots, \tag{B52}$$

where

$$W_+ = \psi_0\left(i\tilde{\omega} - \frac{4\tilde{k}^2}{12+3\tilde{q}^2}\right) + \mathcal{O}(\tilde{\omega}^2, \tilde{\omega}\tilde{k}^2, \tilde{k}^4), \tag{B53a}$$

$$W_- = -X_0 + \mathcal{O}(\tilde{\omega}^2, \tilde{\omega}\tilde{k}^2, \tilde{k}^4), \tag{B53b}$$

$$D_+ = \psi_0 + \mathcal{O}(\tilde{\omega}, \tilde{k}^4), \tag{B53c}$$

$$D_- = X_0\left(-\frac{4\tilde{q}^2}{12+3\tilde{q}^2} + i\tilde{\omega}\frac{(\tilde{q}^2-12)^2}{(12+3\tilde{q}^2)^2} - \tilde{k}^2\frac{32\tilde{q}^4(36+\tilde{q}^2)}{(12+3\tilde{q}^2)^4}\right) + \mathcal{O}\big(\tilde{\omega}^2, \tilde{\omega}\tilde{k}^2, \tilde{k}^4\big). \tag{B53d}$$

Then (B51) implies

$$W_\pm = -C_\pm a_x^{(0)} + \tilde{k}^2 h_t^{x(0)} + i\tilde{k}\tilde{\omega}\chi^{(0)} + \mathcal{O}(\tilde{\omega}^2, \tilde{\omega}\tilde{k}^2, \tilde{k}^4), \tag{B54}$$

therefore

$$\psi_0 = \frac{-C_+ a_x^{(0)} + \tilde{k}^2 h_t^{x(0)} + i\tilde{k}\tilde{\omega}\chi^{(0)} + \mathcal{O}(\tilde{\omega}^2, \tilde{\omega}\tilde{k}^2, \tilde{k}^4)}{i\tilde{\omega} - \tilde{k}^2\frac{4}{12+3\tilde{q}^2} + \mathcal{O}(\tilde{\omega}^2, \tilde{\omega}\tilde{k}^2, \tilde{k}^4)}, \tag{B55}$$

$$X_0 = C_- a_x^{(0)} - \tilde{k}^2 h_t^{x(0)} - i\tilde{k}\tilde{\omega}\chi^{(0)} + \mathcal{O}(\tilde{\omega}^2, \tilde{\omega}\tilde{k}^2, \tilde{k}^4). \tag{B56}$$

From (B25) we can solve for a_x:

$$a_x = \rho\frac{\phi_- - \phi_+}{C_- - C_+}, \tag{B57}$$

which implies

$$a_x'(0) = \frac{D_- - D_+}{C_- - C_+}, \tag{B58}$$

where $D_\pm$ are given in (B53). Using also (B26), we obtain the terms relevant to the electric conductivity

$$\delta a_x'(0)/\delta a_x^{(0)} = -\frac{4i\tilde{\omega}\tilde{q}^2 + \mathcal{O}(\tilde{\omega}^2, \tilde{\omega}\tilde{k}^2)}{(12+3\tilde{q}^2)i\tilde{\omega} - 4\tilde{k}^2 + \mathcal{O}(\tilde{\omega}^2, \tilde{\omega}\tilde{k}^2, \tilde{k}^4)} + i\tilde{\omega}\frac{(12-\tilde{q}^2)^2}{(12+3\tilde{q}^2)^2} + \mathcal{O}(\tilde{\omega}^2, \tilde{\omega}\tilde{k}^2). \tag{B59}$$

To obtain the conductivity, we divide (B59) by $i\tilde{\omega}$. Note that in the fist term and in the numerator of the first term, the terms of order $\tilde{k}^2$ cancel out. This must also be true for terms of order $\tilde{k}^4$, $\tilde{k}^6$ and so on. This is consistent with the fact that the conductivity has no $1/\tilde{\omega}$ poles.

The conductivity is, therefore,

$$\sigma(\tilde{\omega}) = \frac{\tilde{q}^2 + \mathcal{O}(\tilde{\omega}, \tilde{k}^2)}{\tilde{k}^2 - \frac{(12+3\tilde{q}^2)}{4}i\tilde{\omega} + \mathcal{O}(\tilde{\omega}^2, \tilde{\omega}\tilde{k}^2, \tilde{k}^4)} + \frac{(12-\tilde{q}^2)^2}{(12+3\tilde{q}^2)^2} + \mathcal{O}(\tilde{\omega}, \tilde{k}^2). \tag{B60}$$

Now using (B21) we can write (B60) as follows:

$$\sigma(\tilde{\omega}) = \frac{D}{\Gamma - i\tilde{\omega}} + \sigma_Q, \tag{B61}$$

where

$$D = \frac{4\tilde{q}^2}{12+3\tilde{q}^2}, \quad \Gamma = \frac{\tilde{k}^2}{\tilde{q}^2}D, \quad \sigma_Q = \left(\frac{12-\tilde{q}^2}{12+3\tilde{q}^2}\right)^2. \tag{B62}$$

For completeness, we should mention that to obtain the correct conductivity in the limit $\omega \to 0$, we also need the term of order $\mathcal{O}(\tilde{\omega}\tilde{k}^2)$ in the numerator of the second term in (B59). The result was calculated in [71] and is the following:

$$\sigma(\tilde{\omega}) = \frac{D + \Gamma(1-\sigma_Q)}{\Gamma - i\tilde{\omega}} + \sigma_Q. \tag{B63}$$

[14]There are no logarithms in the expansion; one can check from the solution that $\phi_\pm'$ do not contain any $1/\rho$ terms.

[1] K. G. Wilson and M. E. Fisher, Critical Exponents in 3.99 Dimensions, Phys. Rev. Lett. **28**, 240 (1972).

[2] T. Banks and A. Zaks, On the phase structure of vector-like gauge theories with massless fermions, Nucl. Phys. B **196**, 189 (1982).

[3] P. W. Anderson, *Basic Notions of Condensed Matter Physics* (Addison-Wesley, Boston, 1984).

[4] J. Zaanen, Superconductivity: Why the temperature is high? Nature **430**, 512 (2004).

[5] J. Zaanen, A modern, but way too short history of the theory of superconductivity at a high temperature, arXiv:1012.5461.

[6] B. Keimer, S. A. Kivelson, M. R. Norman, S. Uchida, and J. Zaanen, High temperature superconductivity in the cuprates, arXiv:1409.4673.

[7] N. E. Hussey, Phenomenology of the normal state in-plane transport properties of high-T_c cuprates, J. Phys.: Condens. Matter **20**, 123201 (2008).

[8] T. R. Chien, Z. Z. Wang, and N. P. Ong, Effect of Zn Impurities on the Normal-State Hall Angle in Single-Crystal $YBa_2Cu_{3-x}Zn_xO_{7-\delta}$, Phys. Rev. Lett. **67**, 2088 (1991).

[9] H. Takagi, B. Batlogg, H. L. Kao, J. Kwo, R. J. Cava, J. J. Krajewski, and W. F. Peck, Jr., Systematic Evolution

of Temperature-Dependent Resistivity in $La_{2-x}Sr_xCuO_4$, Phys. Rev. Lett. **69**, 2975 (1992).

[10] S. H. Naqib, J. R. Cooper, J. L. Tallon, and C. Panagopoulos, Temperature dependence of electrical resistivity of high-T_c cuprates - from pseudogap to overdoped regions, Physica C **387**, 365 (2003).

[11] R. A. Cooper *et al.*, Anomalous criticality in the electrical resistivity of $La_{2-x}Sr_xCuO_4$, Science **323**, 603 (2009).

[12] N. E. Hussey, R. A. Cooper, Xiaofeng Xu, Y. Wang, I. Mouzopoulou, B. Vignolle, and C. Proust, Dichotomy in the T-linear resistivity in hole-doped cuprates, Philos. Trans. R. Soc. London A **369**, 1626 (2011).

[13] R. Daou, N. Doiron-Leyraud, D. LeBoeuf, S. Y. Li, F. Laliberté, O. Cyr-Choinière, Y. J. Jo, L. Balicas, J.-Q. Yan, J.-S. Zhou, J. B. Goodenough, and L. Taillefer, Linear temperature dependence of resistivity and change in the Fermi surface at the pseudogap critical point of a high-T_c superconductor, Nat. Phys. **5**, 31 (2009).

[14] A. Legros *et al.*, Universal T-linear resistivity and Planckian dissipation in overdoped cuprates, Nat. Phys. **15**, 142 (2019).

[15] S. Zaum, K. Grube, R. Schäfer, E. D. Bauer, J. D. Thompson, and H. V. Löhneysen, Towards the Identification of a Quantum Critical Line in the (p, B) Phase Diagram of $CeCoIn_5$ with Thermal-Expansion Measurements, Phys. Rev. Lett. **106**, 087003 (2011).

[16] A. Shekhter *et al.*, Bounding the pseudogap with a line of phase transitions in $YBa_2Cu_3O_{6+x}$, Nature **498**, 75 (2013).

[17] C. Kendziora, D. Mandrus, L. Mihaly, and L. Forro, Single-band model for the temperature-dependent Hall coefficient of high-T_c superconductors, Phys. Rev. B **46**, 14297 (1992).

[18] H. Y. Hwang, B. Batlogg, H. Takagi, H. L. Kao, J. Kwo, R. J. Cava, J. J. Krajewski, and W. F. Peck, Jr., Scaling of the Temperature Dependent Hall Effect in $La_{2-x}Sr_xCuO_4$, Phys. Rev. Lett. **72**, 2636 (1994).

[19] J. M. Harris, Y. F. Yan, P. Matl, N. P. Ong, P. W. Anderson, T. Kimura, and K. Kitazawa, Violation of Kohler's Rule in the Normal-State Magnetoresistance of $YBa_2Cu_3O_{7-\delta}$ and $La_2Sr_xCuO_4$, Phys. Rev. Lett. **75**, 1391 (1995).

[20] N. E. Hussey, J. R. Cooper, J. M. Wheatley, I. R. Fisher, A. Carrington, A. P. Mackenzie, C. T. Lin, and O. Milat, Angular Dependence of the c-axis Normal State Magnetoresistance in Single Crystal $Tl_2Ba_2CuO_6$, Phys. Rev. Lett. **76**, 122 (1996).

[21] A. P. Mackenzie, S. R. Julian, D. C. Sinclair, and C. T. Lin, Normal-state magnetotransport in superconducting $Tl_2Ba_2CuO_{6+\delta}$ to millikelvin temperatures, Phys. Rev. B **53**, 5848 (1996).

[22] A. W. Tyler and A. P. Mackenzie, Hall effect of single layer, tetragonal $Tl_2Ba_2CuO_{6+\delta}$ near optimal doping, Physica C **282-287**, 1185 (1997).

[23] A. W. Tyler, Y. Ando, F. F. Balakirev, A. Passner, G. S. Boebinger, A. J. Schofield, A. P. Mackenzie, and O. Laborde, High-field study of normal-state magnetotransport in $Tl_2Ba_2CuO_{6+\delta}$, Phys. Rev. B **57**, R728 (1998).

[24] Y. Nakajima, K. Izawa, Y. Matsuda, S. Uji, T. Terashima, H. Shishido, R. Settai, Y. Onuki, and H. Kontani, Normal-state Hall angle and magnetoresistance in quasi-2D heavy fermion $CeCoIn_5$ near a quantum critical point, J. Phys. Soc. Jpn. **73**, 5 (2004).

[25] B. Fauqué, Y. Sidis, V. Hinkov, S. Pailhès, C. T. Lin, X. Chaud, and Ph. Bourges, Magnetic Order in the Pseudogap Phase of High-T_C Superconductors, Phys. Rev. Lett. **96**, 197001 (2006).

[26] Y. Li, V. Balédent, N. Barisic, Y. Cho, B. Fauqué, Y. Sidis, G. Yu, X. Zhao, P. Bourges, and M. Greven, Nature of the enigmatic pseudogap state: novel magnetic order in superconducting $HgBa_2CuO_{4+d}$, Nature **455**, 372 (2008).

[27] F. F. Balakirev, J. B. Betts, A. Migliori, I. Tsukada, Y. Ando, and G. S. Boebinger, Quantum Phase Transition in the Magnetic-Field-Induced Normal State of Optimum-Doped High-T_c Cuprate Superconductors at Low Temperatures, Phys. Rev. Lett. **102**, 017004 (2009).

[28] I. M. Hayes *et al.*, Scaling between magnetic field and temperature in the high-temperature superconductor $BaFe_2(As_{1-x}P_x)_2$, Nat. Phys. **12**, 916 (2016).

[29] S. Licciardello *et al.*, Coexistence of orbital and quantum critical magnetoresistance in $FeSe_{1-x}S_x$, Phys. Rev. Research **1**, 023011 (2019) .

[30] P. Giraldo-Gallo *et al.*, Scale-invariant magnetoresistance in a cuprate superconductor, Science **361**, 479 (2018).

[31] D. van de Marel *et al.*, Quantum critical behavior in a high-T_c superconductor, Nature **425**, 271 (2003).

[32] P. Limelette *et al.*, Phys. Rev. B **87**, 035102 (2013).

[33] L. Prochaska *et al.*, Singular charge fluctuations at a magnetic quantum critical point, Science **367**, 285 (2020).

[34] J. M. Maldacena, The large-N limit of superconformal field theories and supergravity, Int. J. Theor. Phys. **38**, 1113 (1999); The large N limit of superconformal field theories and supergravity, Adv. Theor. Math. Phys. **2**, 231 (1998).

[35] C. Charmousis, B. Goutéraux, B. S. Kim, E. Kiritsis, and R. Meyer, Effective holographic theories for low-temperature condensed matter systems, J. High Energy Phys. 11 (2010) 151.

[36] B. Goutéraux and E. Kiritsis, Generalized holographic quantum criticality at finite density, J. High Energy Phys. 12 (2011) 036.

[37] B. Goutéraux and E. Kiritsis, Quantum critical lines in holographic phases with (un)broken symmetry, J. High Energy Phys. 04 (2013) 053.

[38] B. Gouteraux, Universal scaling properties of extremal cohesive holographic phases, J. High Energy Phys. 01 (2014) 080.

[39] A. Donos, B. Goutéraux, and E. Kiritsis, Holographic metals and insulators with helical symmetry, J. High Energy Phys. 09 (2014) 038.

[40] E. Kiritsis and V. Niarchos, The holographic quantum effective potential at finite temperature and density, J. High Energy Phys. 08 (2012) 164.

[41] S. A. Hartnoll, Lectures on holographic methods for condensed matter physics, Classical Quantum Gravity **26**, 224002 (2009).

[42] C. P. Herzog, Lectures on holographic superfluidity and superconductivity, J. Phys. A **42**, 343001 (2009).

[43] S. Sachdev, Condensed matter and AdS/CFT, Lect. Notes Phys. **828**, 273 (2011).

[44] S. A. Hartnoll, A. Lucas, and S. Sachdev, *Holographic Quantum Matter* (MIT Press, 2018).

[45] J. Zaanen, Y. W. Sun, Y. Liu, and K. Schalm, *Holographic Duality in Condensed Matter Physics* (Cambridge University Press, Cambridge, England, 2015).

[46] M. Ammon and J. Erdmenger, *Gauge/Gravity Duality* (Cambridge University Press, Cambridge, England, 2015).
[47] H. Nastase, *String Theory Methods for Condensed Matter Physics* (Cambridge University Press, Cambridge, England, 2017).
[48] E. Kiritsis, *String Theory in a Nutshell*, 2nd ed. (Princeton University Press, Princeton, NJ, 2019), p. 888.
[49] J. Zaanen, Planckian dissipation, minimal viscosity and the transport in cuprate strange metals, SciPost Phys. **6**, 061 (2019).
[50] H. Liu, J. McGreevy, and D. Vegh, Non-Fermi liquids from holography, Phys. Rev. D **83**, 065029 (2011); T. Faulkner, H. Liu, J. McGreevy, and D. Vegh, Emergent quantum criticality, Fermi surfaces, and AdS_2, *ibid.* **83**, 125002 (2011).
[51] M. Cubrovic, J. Zaanen, and K. Schalm, String theory, quantum phase transitions and the emergent fermi-liquid, Science **325**, 439 (2009).
[52] C. M. Varma *et al.*, Phenomenology of the Normal State of Cu-O High-Temperature Superconductors, Phys. Rev. Lett. **63**, 1996 (1989); **64**, 497(E) (1990); C. M. Varma, Phenomenological constraints on theories for high temperature superconductivity, Int. J. Mod. Phys. **3**, 2083 (1989).
[53] S. A. Hartnoll, J. Polchinski, E. Silverstein, and D. Tong, Towards strange metallic holography, J. High Energy Phys. 04 (2010) 120.
[54] B. S. Kim, E. Kiritsis, and C. Panagopoulos, Holographic quantum criticality and strange metal transport, New J. Phys. **14**, 043045 (2012).
[55] S. S. Pal, Model building in AdS/CMT: DC conductivity and Hall angle, Phys. Rev. D **84**, 126009 (2011).
[56] E. Kiritsis and L. Li, Quantum criticality and DBI magnetoresistance, J. Phys. A **50**, 115402 (2017); S. Cremonini, A. Hoover, and L. Li, Backreacted DBI magnetotransport with momentum dissipation, J. High Energy Phys. 10 (2017) 133.
[57] M. R. Norman and A. V. Chubukov, High-frequency behavior of the infrared conductivity of cuprates, Phys. Rev. B **73**, 140501(R) (2006).
[58] R. A. Davison, B. Goutéraux, and S. A. Hartnoll, Incoherent transport in clean quantum critical metals, J. High Energy Phys. 10 (2015) 112
[59] J. Bhattacharya, S. Cremonini, and B. Goutéraux, Intermediate scalings in holographic RG flows and conductivities, J. High Energy Phys. 02 (2015) 035.
[60] E. Kiritsis and F. Peña-Benitez, Scaling of the holographic AC conductivity for non-Fermi liquids at criticality, J. High Energy Phys. 11 (2015) 177.
[61] A. Karch, K. Limtragool, and P. W. Phillips, Unparticles and anomalous dimensions in the cuprates, J. High Energy Phys. 03 (2016) 175.
[62] R. A. Davison, S. A. Gentle, and B. Goutéraux, Slow Relaxation and Diffusion in Holographic Quantum Critical Phases, Phys. Rev. Lett. **123**, 141601 (2019).
[63] R. A. Davison, S. A. Gentle, and B. Goutéraux, Impact of irrelevant deformations on thermodynamics and transport in holographic quantum critical states, Phys. Rev. D **100**, 086020 (2019).
[64] E. Kiritsis and L. Li, Holographic competition of phases and superconductivity, J. High Energy Phys. 01 (2016) 147.
[65] T. Andrade and B. Withers, A simple holographic model of momentum relaxation, J. High Energy Phys. 05 (2014) 101.
[66] A. Donos and J. P. Gauntlett, Holographic Q-lattices, J. High Energy Phys. 04 (2014) 040.
[67] B. Goutéraux, Charge transport in holography with momentum dissipation, J. High Energy Phys. 04 (2014) 181.
[68] R. A. Davison and B. Goutéraux, Momentum dissipation and effective theories of coherent and incoherent transport, J. High Energy Phys. 01 (2015) 039.
[69] E. Kiritsis and J. Ren, On holographic insulators and supersolids, J. High Energy Phys. 09 (2015) 168.
[70] D. T. Son and A. O. Starinets, Minkowski-space correlators in AdS/CFT correspondence: recipe and applications, J. High Energy Phys. 09 (2002) 042.
[71] R. A. Davison and B. Goutéraux, Dissecting holographic conductivities, J. High Energy Phys. 09 (2015) 090.
[72] D. M. Eagles, Possible pairing without superconductivity at low carrier concentration in bulk and thin-film superconducting semiconductors, Phys. Rev. **186**, 456 (1969); A. J. Leggett, in *Modern Trends in the Theory of Condensed Matter* (Springer, Berlin, 1980); P. Nozières and S. Schmitt Rink, Bose condensation in an attractive fermion gas: from weak to strong coupling superconductivity, J. Low Temp. Phys. **59**, 195 (1985).
[73] T. Enss and J. H. Thywissen, Universal spin transport and quantum bounds for unitary fermions, Annu. Rev. Condens. Matter Phys. **10**, 85 (2019).
[74] K. M. O Hara, A. Altmeyer, S. Riedl, S. Jochim, C. Chin, J. H. Denschlag, and R. Grimm, Observation of a strongly interacting degenerate Fermi gas of atoms, Science **298**, 2179 (2002); C. A. Regal, M. Greiner, and D. S. Jin, Observation of Resonance Condensation of Fermionic Atom Pairs, Phys. Rev. Lett. **92**, 040403 (2004); M. Bartenstein *et al.*, Crossover from a Molecular Bose-Einstein Condensate to a Degenerate Fermi Gas, *ibid.* **92**, 120401 (2004); M. W. Zwierlein, C. A. Stan, C. H. Schunck, S. M. F. Raupach, A. J. Kerman, and W. Ketterle, Condensation of Pairs of Fermionic Atoms near a Feshbach Resonance, *ibid.* **92**, 120403 (2004); J. Kinast, S. L. Hemmer, M. E. Gehm, A. Turlapov, and J. E. Thomas, Evidence for Superfluidity in a Resonantly Interacting Fermi Gas, *ibid.* **92**, 150402 (2004); T. Bourdel, L. Khaykovich, J. Cubizolles, J. Zhang, F. Chevy, M. Teichmann, L. Tarruell, S. J. J. M. F. Kokkelmans, and C. Salomon, Experimental Study of the BEC-BCS Crossover Region in Lithium 6, *ibid.* **93**, 050401 (2004).
[75] T. Enss and R. Haussmann, Quantum Mechanical Limitations to Spin Diffusion in the Unitary Fermi Gas, Phys. Rev. Lett. **109**, 195303 (2012).
[76] T. Stauber, N. M. R. Peres, and A. K. Geim, Optical conductivity of graphene in the visible region of the spectrum, Phys. Rev. B **78**, 085432 (2008); B. Roy, V. Juricic, and S. Das Sarma, Universal optical conductivity of a disordered Weyl semimetal, Sci. Rep. **6**, 32446 (2016); P. Hosur, S. A. Parameswaran, and A. Vishwanath, Charge Transport in Weyl Semimetals Phys. Rev. Lett. **108**, 046602 (2012).
[77] K. F. Mak *et al.*, Measurement of the Optical Conductivity of Graphene, Phys. Rev. Lett. **101**, 196405 (2008); D. Neubauer *et al.*, Optical conductivity of the Weyl semimetal NbP,

Phys. Rev. B **98**, 195203 (2018); B. Xu *et al.*, Optical spectroscopy of the Weyl semimetal TaAs, *ibid.* **93**, 121110(R) (2016); P. Gallagher, C.-S. Yang, T. Lyu, F. Tian, R. Kou, H. Zhang, K. Watanabe, T. Taniguchi, and F. Wang, Quantum-critical conductivity of the Dirac fluid in graphene, Science **364**, 158 (2019).

[78] D. T. Son, Toward an AdS/cold atoms correspondence: A Geometric realization of the Schrodinger symmetry, Phys. Rev. D 78, 046003 (2008).

[79] G. Grignani, A. Marini, F. Peña-Benitez, and S. Speziali, AC conductivity for a holographic Weyl semimetal, J. High Energy Phys. 03 (2017) 125.

[80] K. Y. Kim, K. K. Kim, Y. Seo, and S. J. Sin, Coherent/incoherent metal transition in a holographic model, J. High Energy Phys. 12 (2014) 170.

[81] X. H. Ge, K. Jo, and S. J. Sin, Hydrodynamics of RN AdS_4 black hole and holographic optics, JHEP (2011) 104.